Bulletin of the Seismological Society of America, Vol. 93, No. 2, pp. 870–881, April 2003

Ⓔ

Visualization of 3D Wave Propagation from the 2000 Tottori-ken Seibu, Japan, Earthquake: Observation and Numerical Simulation

by T. Furumura, B. L. N. Kennett, and K. Koketsu

Abstract The dense networks of strong-ground-motion instruments in Japan (K-NET and KiK-net) provide a means of direct visualization of regional wave propagation during large earthquakes. For the 2000 Tottori-ken Seibu earthquake (M_w 6.6) in western Japan, snapshots of ground motion, derived directly from interpolation of a large number of array observations, demonstrate clearly the nature of the source radiation and the character of the seismic wave field propagating to regional distances. In western Japan the wave field from the earthquake is characterized, in most parts, by the dominance of high-frequency (0.2–5 Hz) *Lg* waves on three-component acceleration records and longer-period ($T \sim 10$ sec) fundamental-mode Love waves in tangential displacement. The presence of strong lateral variations in the crust and upper-mantle structures, such as the low-velocity superficial layer and the high-velocity Philippine Sea plate with shallow subduction into the mantle, impose significant modifications on the regional wave field. Further insight into the nature of the seismic wave field is gained by comparison of the observations with numerical simulation for a 3D model, including sedimentary basins by an embedded submesh. A multigrid, parallel computation using a hybrid Pseudospectral/Finite Difference Method allows the inclusion of a realistic model of the source process for the 2000 Tottori-Ken Seibu earthquake. There is good agreement in the dominant features of the regional wave field propagating through the complex structure of western Japan. However, the differences between the observations and the computer simulations indicates the need for further refinement of the source and structural models. The inclusion of amplification effects for the population centers in sedimentary basins means that the modeling procedure is already suitable for estimating the main pattern of ground motion for future earthquake scenarios.

Online material: MPEG movies of observed and simulated wave fields.

Introduction

During the past few years very dense arrays of strong-ground-motion instruments have been deployed across Japan by the National Research Institute for Earth Science and Disaster Prevention (NIED). The combination of the K-NET (Kinoshita, 1998) and the KiK-net (Aoi *et al.*, 2000) provides more than 1600 strong motion instruments at a nearly uniform station interval of 10 to 20 km. The development of such a dense array of instruments means that it is now feasible to visualize the behavior of the seismic wave propagation from large earthquakes across the heterogeneous structure of the Japanese Islands.

Huang (2000) may have been the first to use a dense array of strong-ground-motion stations to examine the character of the wave field. He used the 400 stations of the Taiwan national network (Liu *et al.*, 1999) to illustrate the seismic radiation and propagation characteristics during the 1999 Chi-Chi, Taiwan (M_w 7.5) earthquake. Koketsu and Kikuchi (2000) combined data from 400 strong-motion accelerograph and seismic intensity meters in the Kanto, Japan area to study the relation between the complicated wave propagation character of the Love waves and 3D basin structure.

We build on the results of these studies by using the dense network in western Japan to study the nature of the seismic wave field produced by the 2000 Tottori-ken Seibu earthquake (M_w 6.6). This shallow thrust fault event with a hypocentral depth of 11 km was well recorded at 521 K-NET and KiK-net stations with a dense enough spacing to allow interpolation for medium-period waves. Using a combination of snapshots of ground motion and three-component waveforms we show that short-period *Lg* waves (0.2–5 Hz) were the dominant feature in ground acceleration,

whereas ground displacement was dominated by longer-period fundamental-mode Love waves ($T = 10$ sec) on the tangential component. These dominant phases carry a wealth of information about the structure in the crust and upper mantle and can be exploited to extract structural variation; in particular, the phase velocity of the fundamental-mode Love wave was estimated for many stations and used to determine *S*-wave velocity structure.

With the aid of a a newly developed multigrid hybrid Pseudospectral Method (PSM)/Finite Difference Method (FDM) code for parallel computation we are able to compare the observations of ground motion with numerical simulations based on a model of 3D structure and a detailed source-slip model for the earthquake, and thereby seek to improve understanding of the wave field and the structure through which it has passed.

Observations for the 2000 Tottori-ken Seibu Earthquake

The Tottori-ken Seibu earthquake of 16 October 2000 was the largest damaging event since the destructive 1995 Hyogo-ken Nanbu (Kobe) earthquake (M_w 6.9) which also occurred in western Japan. The ground shaking during the 2000 event was well recorded at 521 stations of the new strong-ground-motion networks (Fig. 1) and this allows a good assessment of the wave field from close to the source to regional distances. Each seismic station of the K-NET and the KiK-net consist of a three-component force-balanced accelerograph with a flat response from DC to 30 Hz and a maximum scale of ± 2000 cm/sec^2. The ground acceleration is recorded at 100 or 200 samples/sec with a resolution of 24 bits in analog to digital conversion (Kinoshita, 1998; Aoi *et al.*, 2000).

Snapshots of Ground Motion

Figure 2 shows a set of snapshots of seismic wave propagation during the Tottori-ken Seibu earthquake, produced by spatial interpolation of waveforms from 521 stations (Fig. 1), illustrating the distribution of the horizontal ground velocity motions in both time and space following source initiation. To produce the interpolated wave field, we first integrate the accelerograph to the velocity record after applying the high-pass filter at a cutoff frequency of 0.05 Hz to remove instrumental noise. We also apply a high-cut filter with cutoff frequency of 0.25 Hz to reduce the spatial aliasing effect. The resultant waveforms have a predominant frequency of about 0.1 Hz. With the typical *S*-wave speed of 2.7 km/sec for the shallow structure of western Japan (Ito *et al.*, 1995), this gives a wavelength of about 27 km which is almost twice the mean station interval (about 15 km). The

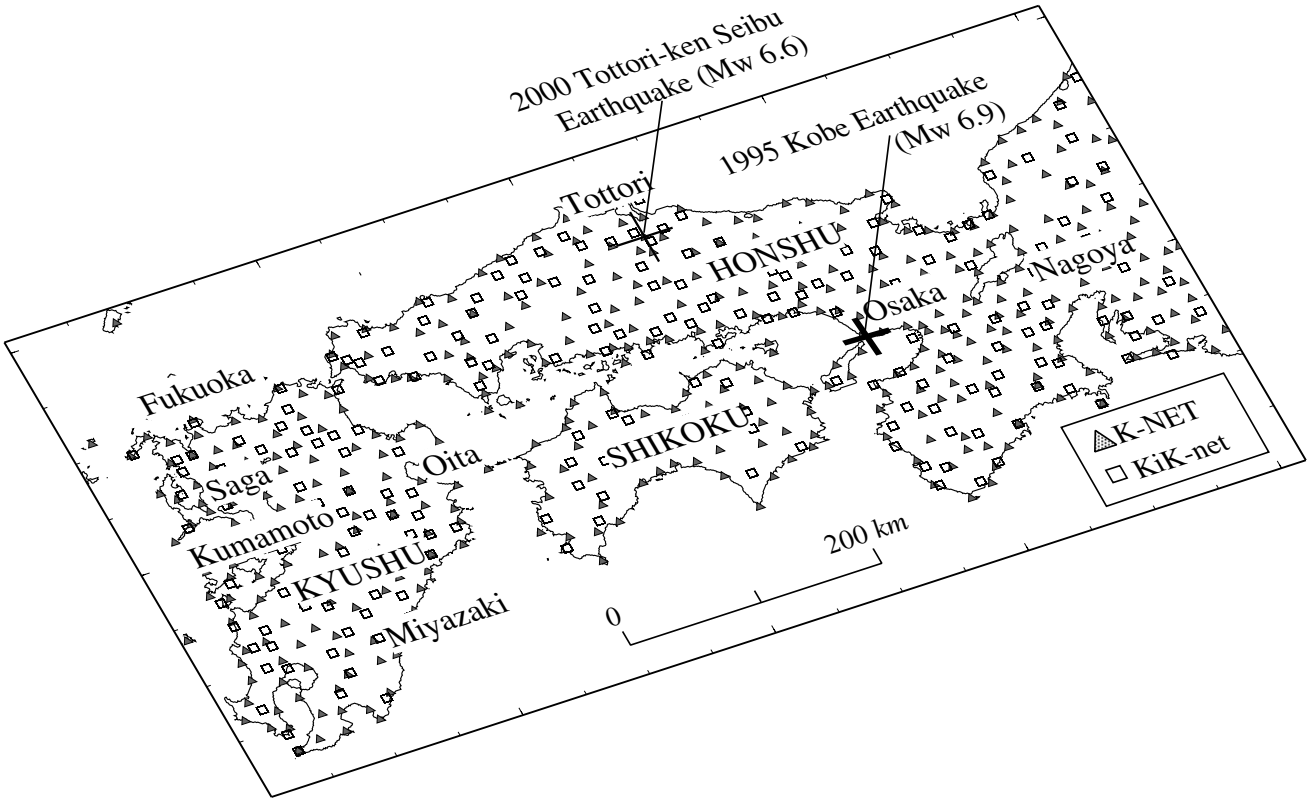

Figure 1. Three-dimensional view of the networks of strong-ground-motion instruments in western Japan which recorded the 2000 Tottori-ken Seibu earthquake. Major features are indicated for reference in later figures with the same view.

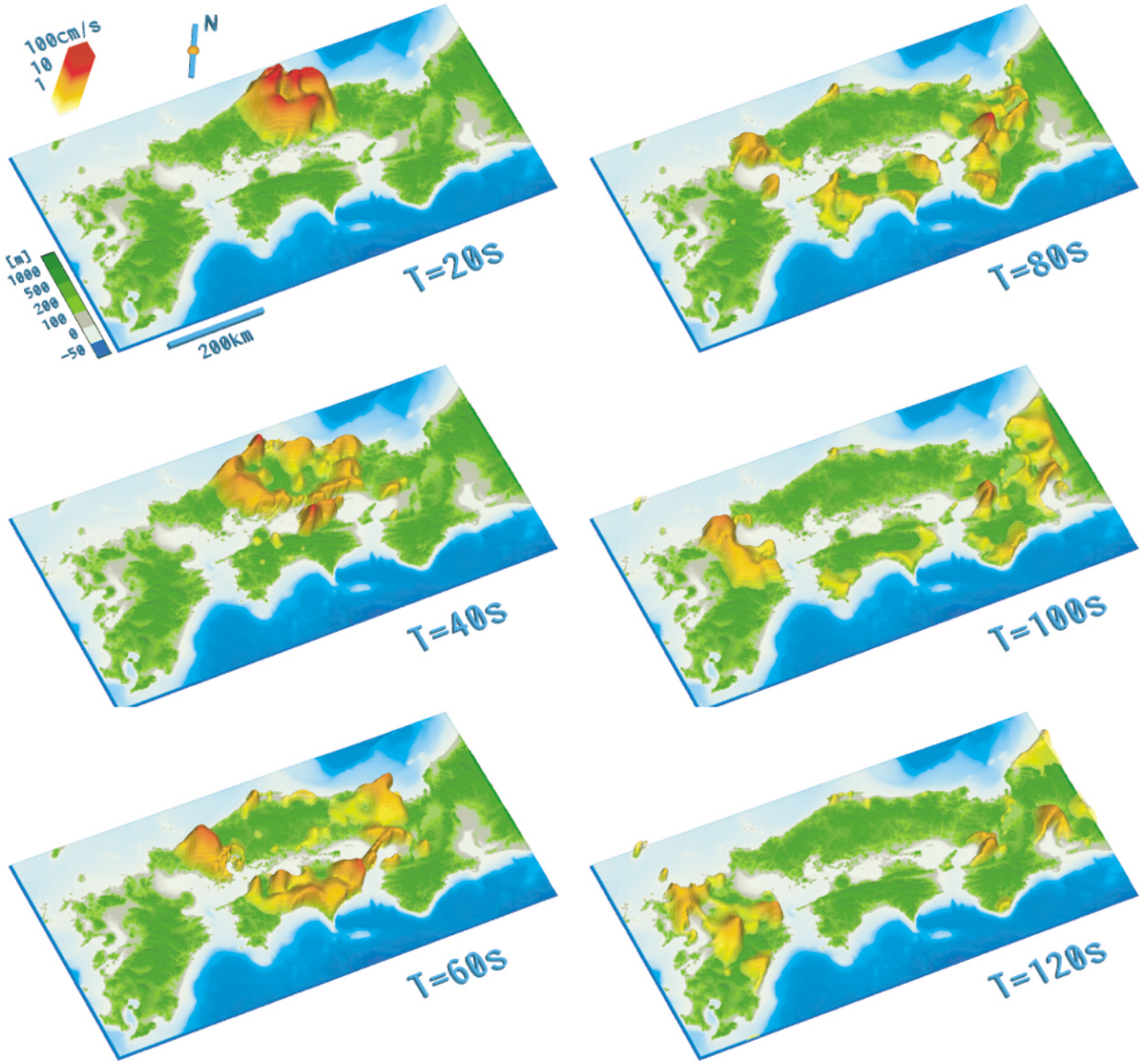

Figure 2. Three-dimensional view of the horizontal ground motions in western Japan during the 2000 Tottori-ken Seibu earthquake, produced by interpolation of velocity waveforms from 521 K-NET and KiK-net stations. The horizontal ground velocity is displayed in a sequence of snapshots at 20-sec intervals, with the time marked below the individual frames. Ground motions outside Japan are masked. The amplitude scale for ground velocity in centimeters per second is shown by a color bar at the top left. (MPEG movie is available online at the SSA website.)

spatial interpolation of waveforms between station at each time step is performed using a gridding algorithm developed by Smith and Wessel (1990).

In the first frame of the snapshot at 20 sec after source initiation, we see that large ground motions with horizontal velocities greater than 20 cm/sec is built up from the radiation produced by the main slip of the source. The longer-period *SH*-wave radiation from the relatively large (M_w 6.6) and shallow (h = 11 km) strike-slip fault source shows a clear four-lobe pattern around the hypocenter. Smaller amplitude *P* waves in north–south and east–west directions can be discerned outside the rampart formed by the large *S* waves (e.g., in the 40 sec frame).

As the waves spread away from the source, multiple reflections of *SH* waves between the free surface and the interfaces in the crust gradually build up the Love waves. The fundamental-mode Love wave at a predominant frequency around 0.1 Hz and phase speed close to 2.8 km/sec is the most prominent feature of the wave field in western Japan. The progression of the Love waves to the west through Honshu to Kyushu is particularly clear in the frames from 40 to 100 sec.

In the later frames the effect of near-surface heterogeneity becomes very apparent and imposes significant modulation on the regional wavefield. The amplification of the ground motions in sedimentary basins, such as at Osaka, Nagoya, and Fukuoka, are very clear in the later snapshots (80, 100 sec). Also, we see large and long duration of ground motions at major basins of Kyushu, such as at Saga, Oita, Kumamoto, and Miyazaki in the 120 sec frame. The larger site amplification at these basins has been reported by Ikeda and Sasatani (1991).

The peak ground velocity in the Osaka basin reaches 2 cm/sec and in the Nagoya basin 1 cm/sec; these values are at least twice as large as in the surrounding areas. The ground oscillation in the basin also continues for several tens of seconds so that the shapes of the basins are clearly outlined in the last two frames (100 and 120 sec).

Peak Ground Acceleration and Displacement

The snapshots in Figure 2 show low-pass-filtered horizontal ground velocity, but it is also important to examine the acceleration and displacement fields. Figure 3a shows the distribution of peak ground acceleration (PGA), and Fig. 3b, the peak ground displacement (PGD) produced by the earthquake. The PGA pattern shows an almost circular distribution around the hypocenter, because the radiation pattern may diminish at high frequencies (e.g., Liu and Helmberger, 1985).

The extension of the isoseismic contours by *SH*-wave radiation is more clearly seen in the PGD map because the longer-period Love wave is enhanced in the displacement response. The ground displacement is used for estimating magnitude (Tsuboi, 1954) by the Japan Meteorological Agency (JMA). For the Tottori-ken Seibu earthquake this magnitude (M_j 7.3) was significantly larger than the moment magnitude (M_w 6.6). The discrepancy appears to arise from the dominance of the Love wave that has a slow rate of decay with epicentral distance compared with that used in the Tsuboi (1954) formula (see also Furumura and Kennett, 2001).

The PGD pattern of Figure 3 also indicates strong control of the ground motion by local conditions. We see some pockets of ground displacement of more than 5 cm, such as in the Oita basin in eastern Kyushu and in the Osaka basin.

Acceleration and Displacement Waveforms

A nearly linear line of stations extending from the epicenter into northern Kyushu have been used to produce three-component record sections. The line of stations is indicated by larger triangles in Figure 3. Records for both ground acceleration and displacements are displayed in Figure 4, and allow the nature of regional wave field in different frequency bands to be contrasted. Because the strong-motion stations rely on triggering, not all records include the *P*-wave arrivals.

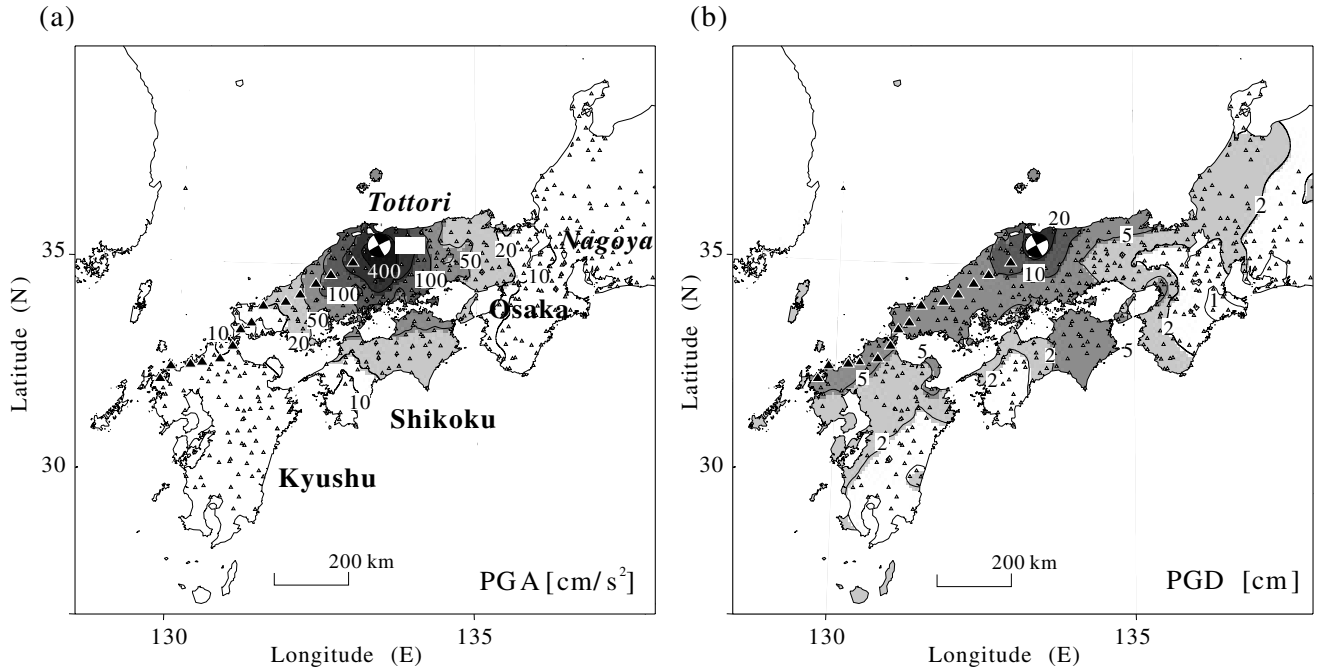

Figure 3. Distribution of (a) peak ground acceleration in centimeters per second squared and (b) displacement in centimeters for the 2000 Tottori-ken Seibu earthquake. The K-NET and the KiK-net stations used in the wavefield reconstruction are shown by triangles. Large solid triangles denote seismic stations whose three-component waveforms are shown in Figure 4.

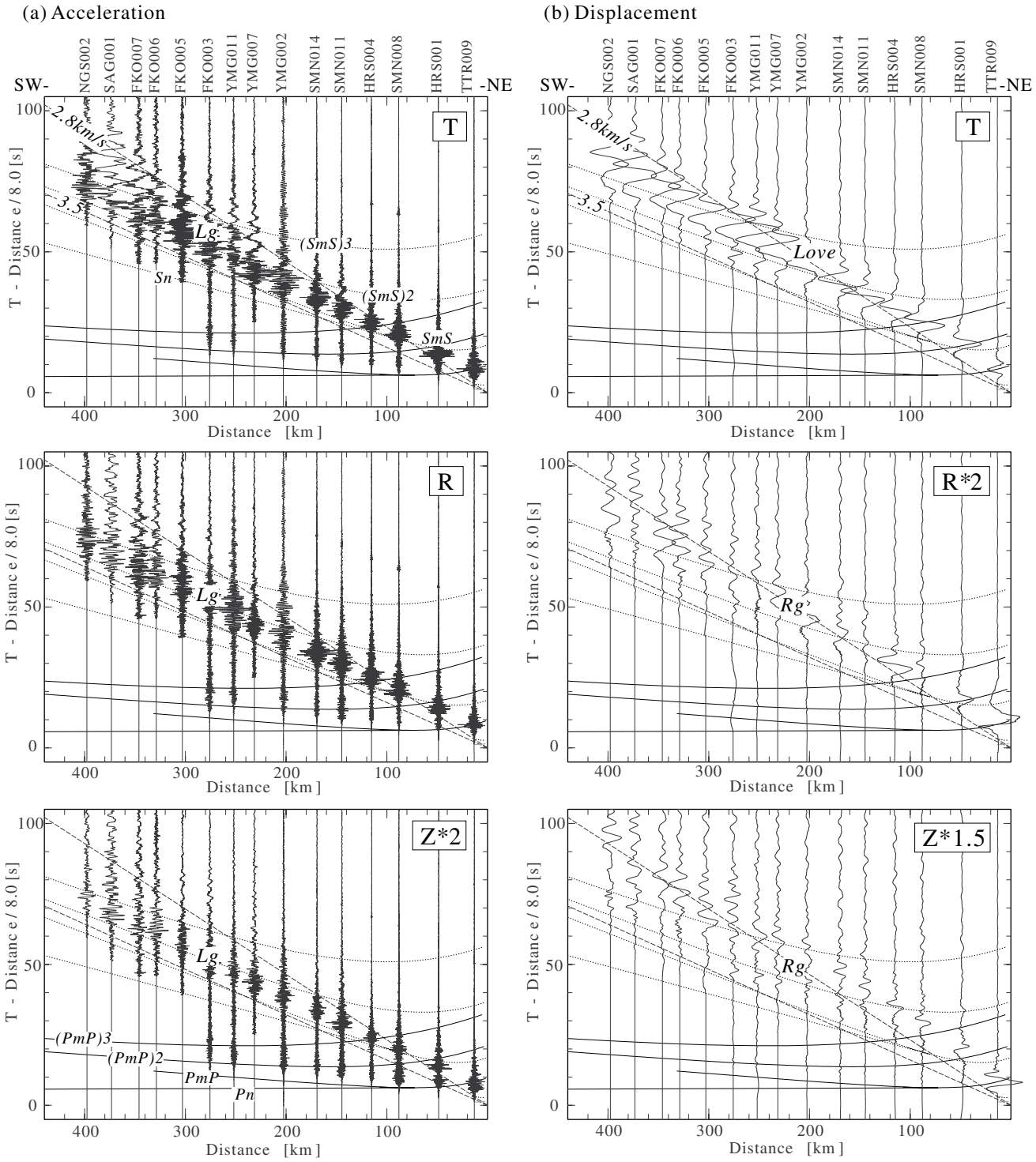

Figure 4. Three-component record sections of (a) ground acceleration and (b) ground displacement from the 2000 Tottori-ken Seibu earthquake derived from KiK-net stations, which major phases marked. The horizontal components have been rotated to radial (*R*) and tangential (*T*) motions relative to the path to the hypocenter. To increase the visibility of the arrivals, the traces are scaled both by epicentral distances and variable scaling is used between components as indicated on each section. The station names are indicated at the top of the sections.

The three-component acceleration waveforms show large-amplitude *Lg* waves at relatively high frequencies extending from about 0.2 to 5 Hz and encompassing a wide range of group velocities from 3.5 to 2.8 km/sec. The *Lg* wave, built up from the superposition of multiple *SmS* reflections in the crustal wave guide, emerges as a distinct packet of arrivals for epicentral distances greater than 150 km and is the largest feature on the traces. Close to the source, the direct *S* makes the main contribution to the PGA pattern seen in Figure 3, but beyond 150 km out to regional distances, the principal contribution is from the *Lg* wave. The efficient propagation of the *Lg* wave in western Japan has been reported by Utsu (1958), Shima (1962), Furumura and Kennett (2001), and Kennett and Furumura (2002).

In some cases, such as stations in sedimentary basins with low velocity and high attenuation, the high-frequency component of *Lg* disappears suddenly. For the western stations near Fukuoka (FKO006, FKO007, SAG001, and NGS002), we find considerable disruption of the *Lg* waves with a noticeable loss of higher frequencies. This effect is most clearly seen on the vertical (*Z*) ground acceleration. Conversions to *P* and *Rg* waves at the edges of basins will tend to reduce the *Lg* amplitude.

The three-component displacement records for the same stations in Figure 4b show a rather different aspect of the wave field. The high-frequency *Lg* waves are overshadowed by the much larger longer-period surface waves. We see a clear fundamental-mode Love wave at a predominant frequency around 0.1 Hz and a group velocity close to 2.8 km/sec in tangential motions. The *Rg* wave (fundamental-mode Rayleigh wave) can be seen on the radial and vertical displacements with group velocity near 2.8 km/sec, but the amplitude is rather small compared with the Love wave on the tangential component. The difference arises because the right lateral strike-slip fault gives much less *SV*-wave radiation in the horizontal plane than the *SH*-wave radiation on the tangential component.

The PGD distribution shown in Figure 3b is therefore dominated by a strong source radiation effect into *SH* waves and Love waves at larger distances. The *SH* waveforms near the source are rather simple, but as the distance increases we see a clear effect of dispersion leading to an elongated Love wave train. The Love waves are noticeably extended at two Kyushu stations (SAG001 and NGS002) where low-velocity sediments overlie bedrock with a large contrast in seismic wavespeeds.

Phase Dispersion of Love Waves

Although there have been extensive studies of *P*-wavespeed structures in western Japan, such as travel-time tomography studies (e.g., Zhao and Hasegawa, 1993) and refraction experiments (e.g., Yoshii *et al.*, 1974), comparatively little attention has been given to the *S*-wavespeed structure. However, recent studies have exploited receiver functions of far-field waveforms (Shibutani, 2001) and tomography using limited *S*-wave arrival-time data (Yoshii *et al.*, 2002). The dense observations of the Tottori-ken Seibu event provide an opportunity to improve knowledge of *S*-wave structure in western Japan.

Because the fundamental-mode Love wave from the event was widely observed with a good signal-to-noise ratio, we can use the dispersion of these waves to estimate the *S*-wave velocity for the crust and upper-mantle structure. The Love waves extend to periods of 30 sec and so provide good control on crustal structure; higher frequency components of the Love wave also improve the resolution of shallow structure.

The phase velocity of the fundamental-mode Love waves has been analyzed in four areas where they were observed with large amplitudes: (A) Fukuoka, (B) Shimane, (C) Maizuru, and (D) Shikoku (see Fig. 5). The phase dispersion is then inverted to estimate 1D *S*-wave structure beneath the groups of stations.

To estimate the phase velocities of the Love wave over a wide frequency range we use a waveform correlation approach. We select five stations in each area to provide a broad range of station separations; the ten station pairs give interstation intervals between 20 and 150 km. A set of narrow bandpass filters, with constant attenuation coefficient, are applied to the Love waves for central frequencies from 0.03 to 0.25 Hz, and the correlation functions of the filtered waveforms are calculated for each pair of stations. The phase velocities are extracted by determining the time lag for maximum coherency in the correlation function between the stations and then dividing by the interstation distance. We do not accept estimates of the phase speed where the wavelength at a given frequency is twice as large as the station separation or where the wavelength is smaller than the station interval. The final result for each group of five stations is obtained by averaging the phase speeds from all the relevant stations pairs to provide a stable estimate of the Love wave dispersion curve in the frequency range from 0.03 to about 0.25 Hz. Careful consideration may be needed for determining the maximum frequency of the phase-velocity measurement, because the phase velocity not only depends on the medium but also on the local geometry of the wave field (see Wielandt, 1993). The accuracy of the phase-velocity measurements using a line array data and its related problems in the inversion study are discussed extensively in Friederich *et al.* (1994).

The resultant dispersion curves of the Love waves for the four areas of A–D are shown in Figure 5, with the error bars denoting one standard deviation from the average phase dispersion curve. In all areas we have normal dispersion with decreasing phase velocities at larger frequencies. The relatively gentle change in the phase velocities for frequencies around 0.1 Hz observed in all areas. This is associated with the prominent arrivals of the Love waves at the frequency of 0.1 Hz in the observed records because the energy in this frequency band is concentrated in time. (See the insert panel of the waveforms for each group of stations in Fig. 5.)

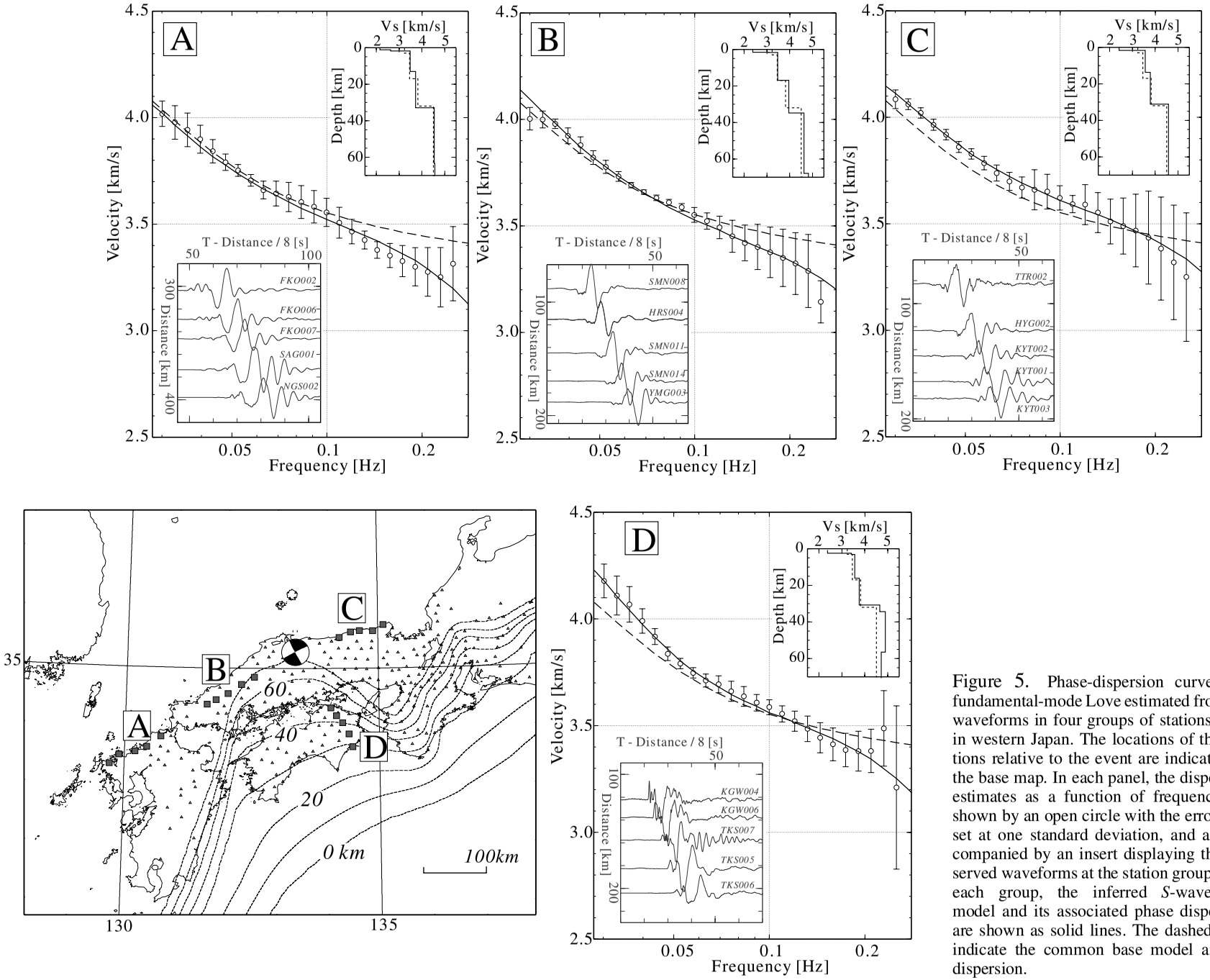

Figure 5. Phase-dispersion curves for fundamental-mode Love estimated from the waveforms in four groups of stations A–D in western Japan. The locations of the stations relative to the event are indicated on the base map. In each panel, the dispersion estimates as a function of frequency are shown by an open circle with the error bars set at one standard deviation, and are accompanied by an insert displaying the observed waveforms at the station groups. For each group, the inferred *S*-wavespeed model and its associated phase dispersion are shown as solid lines. The dashed lines indicate the common base model and its dispersion.

For frequencies higher than 0.2 Hz, the phase speed in all areas is lower than 3.4 km/sec, indicating low-velocity materials in the shallow structure. For area D the phase velocity for frequencies below 0.04 Hz is more than 5% faster than in the other areas; this appears to be related to the shallow subduction of the high-velocity Philippine Sea plate in the uppermost mantle. The scatters in the observations are larger for higher frequencies, especially for areas A and D, where lateral variation in the shallow structure is likely to be significant. For these higher frequencies the excitation of the fundamental-mode Love wave by the source may not be sufficient to suppress the influence of higher Love modes.

The inversion of the phase-dispersion curves to derive the 1D *S*-wavespeed structures in each area was performed using the Genetic Algorithm (GA) (Carroll, 1996) to find a model for which the theoretical dispersion provides a satisfactory match to the observed dispersion curves for the fundamental-mode Love waves. The initial *S*-wave model (indicated by dashed lines in Fig. 5) used for all areas is derived from the *P*-wavespeed model for western Japan (Ito *et al.*, 1995) using a V_p/V_s ratio of 1.73 and a lateral variation of Moho depth (Ryoki, 1999). To account for shallow structure we included two additional shallow layers. The dispersion of the phase speed with frequency is a strongly nonlinear function of the wavespeeds and the thickness of the layers, and so we limit the search space of the GA inversion for the *S* wavespeed to $\pm 20\%$ from the base model. Because the phase velocities are less sensitive to density than the other parameters, we derive the density ρ from the V_s using a simple relation of $\rho = 0.252 + 0.655V_s$ which is derived from the experimental data of Nafe and Drake (1957). The GA inversion uses populations of 20 models at each generation with ordinary GA parameters of 0.02 for the mutation fraction, 0.5 for the crossbar probability, and 0.04 for the creep following the study of Carroll (1996). The experiment is repeated for 50 generations to minimize the sum of residuals between observed and theoretical phase velocities weighted by standard deviations at each frequency.

The *S*-wavespeed models derived from the GA inversion for areas A–D are illustrated in Figure 5 along with the theoretical dispersion curves for the fundamental-mode Love wave. The dispersion for the common initial *S*-wave model is shown in dashed lines for comparison. In northern Kyushu (area A) the surficial layer is both slower (*S*-wave velocity 2.1 km/sec) and thicker (4 km) than in the other areas. The surface *S* wavespeed for regions B–D is about 2.3–2.4 km/sec, and this surface layer is relatively thin for regions B and C in Honshu. The surface layer is somewhat thicker in Shikoku (area D). The high phase speeds at low frequency for area D in Shikoku require the presence of high *S* velocities in the upper mantle. A layer with *S* velocity of 4.9 km/sec and thickness about 20 km is required at a depth of 30 km, which indicates the influence of the shallowly subducting Philippine Sea Plate below the crust.

Numerical Simulation for the 2000 Tottori-ken Seibu Earthquake

Using a detailed 3D subsurface structure and an appropriate source model for the earthquake, we conduct a numerical 3D simulation of the resulting seismic wave propagation and try to reproduce the regional wave field during the 2000 Tottori-ken Seibu earthquake.

The 3D model of *P*-wave structure has been constructed based on the refraction experiments (e.g., Yoshii *et al.*, 1974) and *P*-wave travel-time tomography studies (e.g., Zhao and Hasegawa, 1993). We use the *S*-wave velocity data derived by this study and have constructed a rough 3D model by spatial interpolation between the five stations groups. The averaged 1D structural model is shown in Table 1. The 3D model includes lateral changes in the Moho depth (Ryoki, 1999) and the depth to the top of the Philippine Sea Plate (Yamazaki and Ooida, 1985), as illustrated in Figure 6. The depth of the midcrustal Conrad interface is assumed to lie at half the Moho depth.

To increase the stability of the calculation the water layer is excluded from the model and is replaced by the superficial layers; for the same reason, we exclude the surface topography (less than 2 km across the region) so that the simulations are for a level competent surface. In the sedimentary basins we impose a 2-km-thick layer of lower velocity ($V_s = 2.1$ km/sec) and relatively high attenuation ($Q = 100$).

We use a hybrid PSM/FDM code (Furumura *et al.*, 2000, 2002) for the large scale 3D simulation of seismic waves using a parallel computer. This modeling scheme uses the accurate Fourier PSM in horizontal planes, and a conventional fourth-order FDM in vertical direction with a somewhat smaller mesh increment than horizontal directions. This hybrid scheme minimizes the communication overhead in the parallel computation (Furumura *et al.*, 2002).

To incorporate shallow basin structures in the main 3D simulation model, we embed a finer mesh model at the surface in the coarser main mesh. The wave fields in the two domains are linked by an accurate interpolation procedure. Such a multigrid approach for high-resolution modeling has been successfully employed with the 3D FDM (e.g., Aoi and Fujiwara, 1999; Wang *et al.*, 2001), and is here adapted to PSM calculation with a high-accuracy spatial interpolation

Table 1
The Base Model for Western Japan

	Thickness (km)	V_p (km/sec)	V_s (km/sec)	ρ (t/m^3)	Q
Layer 1 (sediment)	2.0	4.0	2.10	2.0	100
Layer 2	3.0	5.6	3.23	2.5	200
Upper crust	13.0	6.0	3.46	2.7	300
Lower crust	14.0	6.6	3.82	3.0	400
Upper mantle	40.0	7.8	4.50	3.2	500
		8.0	4.62	3.3	500

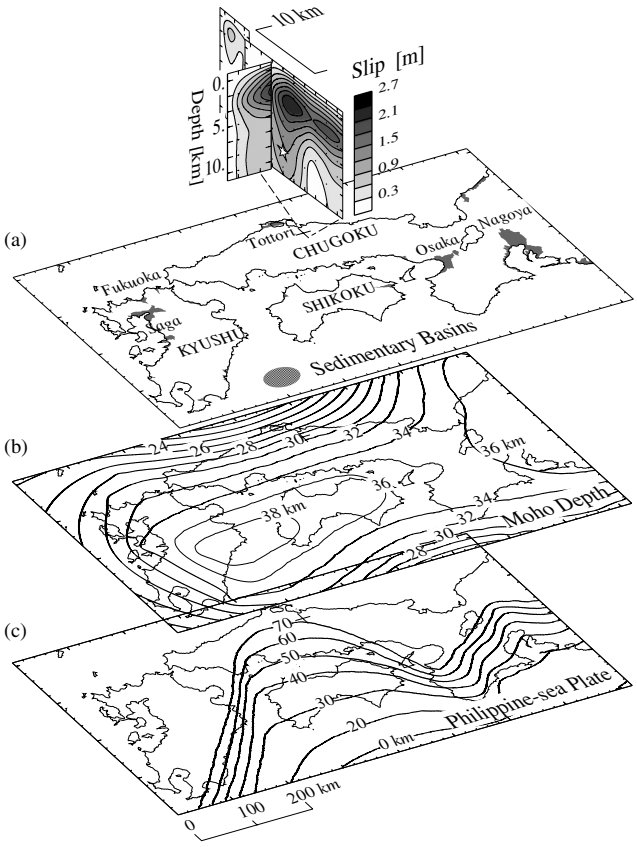

Figure 6. Structural model for western Japan used in the 3D simulation of seismic waves, showing (a) configuration of sedimentary basin, (b) the Moho, and (c) the Philippine Sea plate. The source-slip model of Yagi and Kikuchi (2000) for the 2000 Tottori-ken Seibu earthquake is displayed at the top.

procedure based on the Fourier polynomial extrapolations to connect the two wave fields with different grid sizes.

The simulation model covers a zone of 819 by 409 by 167 km. The model is discretized with a horizontal mesh increment of 1.6 km and a vertical increment of 0.8 km. The embedded finer-mesh model is 4 km thick with a smaller mesh increment of 0.8 by 0.8 by 0.4 km. Using this multigrid model, we can efficiently incorporate smaller-scale near-surface heterogeneities in the large-scale model.

The source model we use is derived from an inversion of strong-motion data from K-NET and KiK-net, with teleseismic waveforms (Yagi and Kikuchi, 2000). The inferred slip distribution is shown in the upper part of Figure 6. The fault model is represented by one large segment of 16 km by 12 km cutting from south to north with two associated small branches to the west and north. On the main segment the fault rupture runs bilaterally from the epicenter with an average speed of 2.5 km/sec, and a large slip of more than 2.5 m occurs at a depth of 5 km above the epicenter.

The source rupture is represented by a set of point sources arranged on the fault plane, which impart seismic wave with a maximum frequency of 1 Hz and a total energy of 1.93×10^{19} Nm for the earthquake. Following Iwata *et al.* (2000) and Horikawa (2000) we use a slightly larger moment than in the original estimate 0.93×10^{19} Nm by Yagi and Kikuchi (2000).

We have assigned a minimum shear-wave velocity of 2.1 km/sec to the sedimentary basins, so that the 3D modeling can accurately treat seismic wave propagation for frequencies below 1 Hz with sampling of 2.6 grid points per shortest wavelength in the horizontal direction and 5.2 grid points in the vertical. The computation was performed on a cluster of four 2.2-GHz Intel Xeon PCs (8 CPUs in total) connected by a Gigabit Ethernet local network. The parallel calculation required 5 GBytes memory and a wall-clock time of 20 hours to march 6000 time steps.

Comparison of Simulation Results and Observations

Figure 7 displays a set of snapshots of horizontal ground velocity derived from the 3D simulation at 20-sec intervals, which should be compared with the corresponding snapshots of the observed ground motions shown in Figure 2. We have imposed the same masking on the calculations as the observations for the area outside Japan and in the marginal seas. This allows a more direct comparison of results.

In the snapshot at 20 sec after the source initiation, the *P* wavefront can be seen as a small outer ring surrounding the large-amplitude *SH* wave. Even though we have used a complex slip model for the event in a moderately complex 3D model, it would appear that the simulated source radiation is somewhat simpler than in the observations. In both source and structural inversions we would expect to emphasize the longer wavelength components and so miss the full complexity of the situation. In the second frame at 40 sec the *Lg* wave begins to separate from the rest of the *S*-wave energy. The *Lg* wave propagates to regional distances at a group velocity close to 3.5 km/sec followed by a large-amplitude fundamental-mode Love wave at 2.8 km/sec.

As the *S* waves propagate further, the effect of shallow-basin structures imposes significant modulation on the wave field. In the numerical simulation we see large ground oscillations for the major population centers such as Nagoya, Osaka, and Fukuoka; this ground shaking in the basins is sustained for several tens of seconds. Such localized amplification effects due to the shallow structures are demonstrated in the present high-resolution simulation using a combined mesh model, but it could not be reproduced in the previous simulation using a coarse mesh model (Kennett and Furumura, 2002).

In the last two snapshots (100, 120 sec) we see the significant disruption of the fundamental-mode Love wave pattern by propagation through the sedimentary basins. The amplitude of the Love waves decrease gradually with propagation in the basin by both dispersion and attenuation in the presence of the low-velocity and high-attenuation materials. Some conversions from fundamental mode to the higher-mode surface waves at the basin edge may also ex-

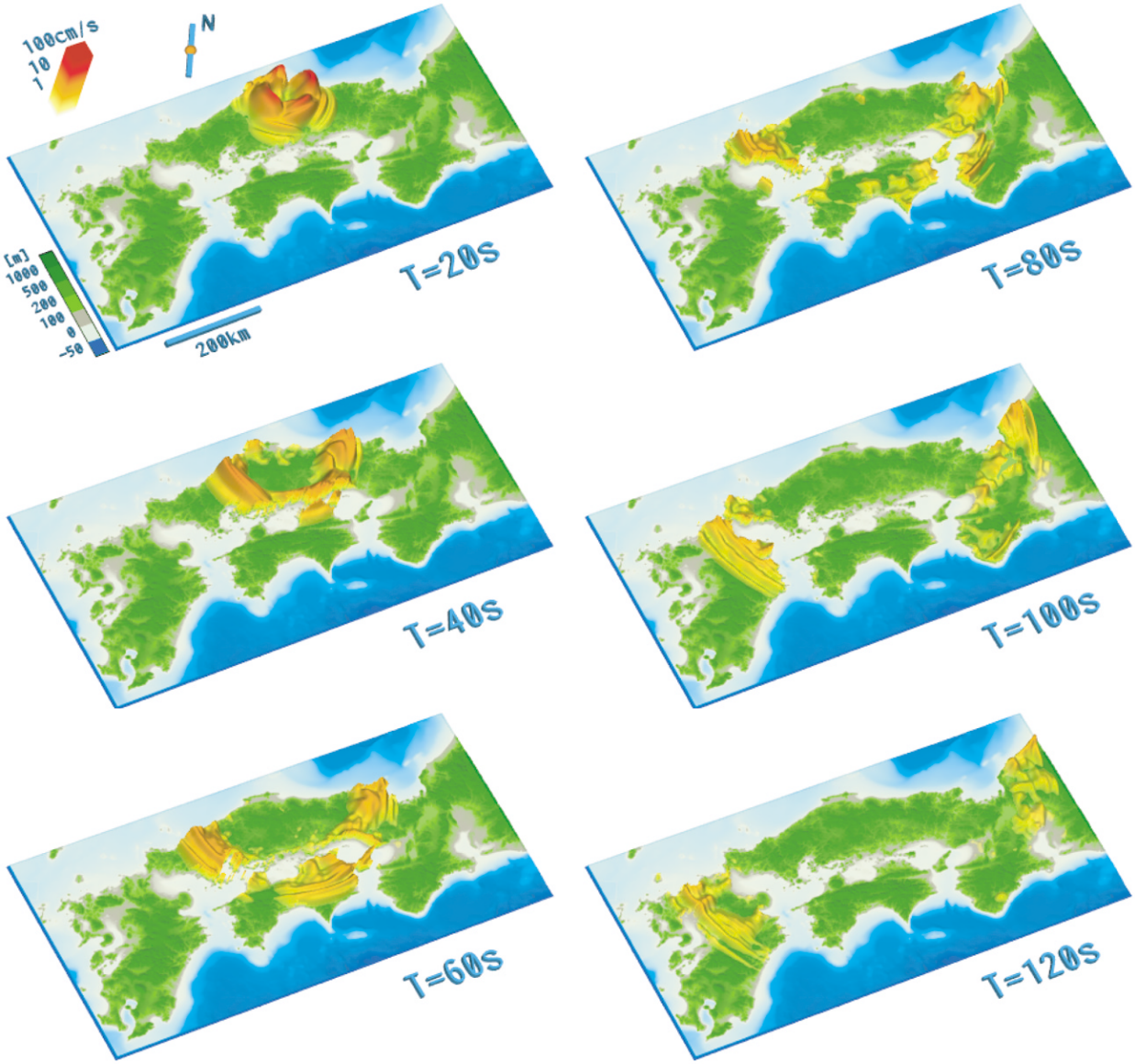

Figure 7. Snapshots of horizontal ground velocity, at 20-sec intervals after source initiation, from 3D numerical simulation of the 2000 Tottori-ken Seibu earthquake in the model shown in Figure 6. (MPEG movies are available online at the SSA website.)

tend the packet of the Love wave. In the last frame (120 sec) we see an elongated and amplified Love wavetrain propagating across the center of Kyushu, but the amplitude is still maintained to large distances.

The peak ground velocity (PGV) patterns derived from the 3D numerical simulation and the observations are compared in Figure 8. To facilitate comparison a low-pass filter with cutoff frequency of 1 Hz has been applied to both the wavefields. The simulated PGV in Figure 8a explains the pattern of observation fairly well with an extension of larger ground motion to the west and south. However, the actual wave field shows more complex patterns, which would suggest a more irregular source-rupture process and smaller-scale heterogeneities in the structure.

We also display in Figure 8 a comparison of simulated and observed waveforms of ground velocity for both tangential and radial components at three KiK-net stations (KYTH02, TKSH02 and SMNH14). These stations were not used in the analysis of phase-speed dispersion to derive the 3D *S*-wavespeed model. The features of the observed velocities in tangential motion are reproduced quite well by the simulations from the arrival of the body *S* wave to the coda of the Love wave. However, there are more differences in the waveforms of radial component ground-velocity motions. The waveshape of the *Rg* is not well recovered and the higher mode Rayleigh waves may be more strongly excited in the simulations than the observations. The differences suggest that a more complex source model is required

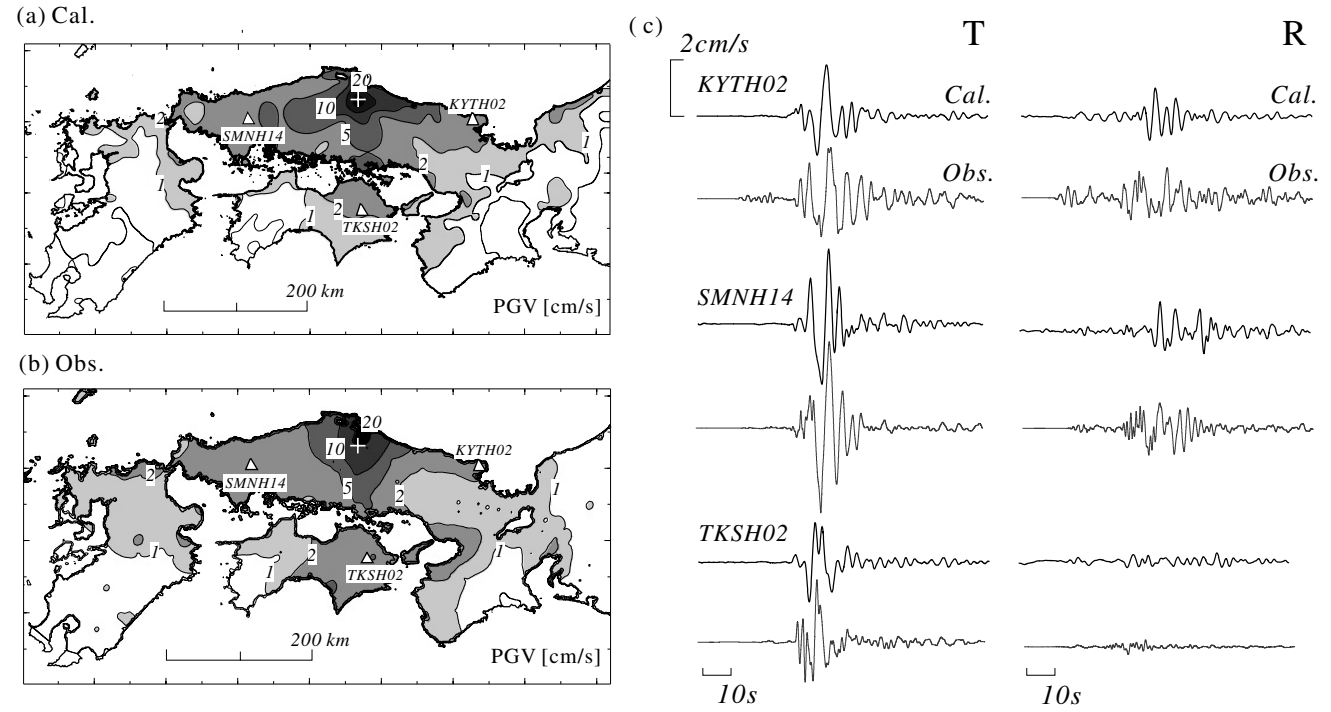

Figure 8. Peak ground displacement of horizontal motion derived from (a) numerical 3D simulation and (b) observations from K-NET and KiK-net stations. (c) Waveforms of tangential (*T*) and radial (*R*) component displacement record derived by simulation (*Cal.*) are compared with observed record (*Obs.*) at three KiK-net stations of KYTH02, SMNH14, and TKSH02.

and also that even more severe shallow attenuation may be needed than is applied in the current model. Clearly it would be desirable to improve the models for shallow structure for both *P* and *S* waves from, for example, dispersion analysis for the *Rg* waves for other events across the region. Local estimates may be obtainable using smaller events recorded at the strong-motion stations.

Conclusions

The character of the regional wavefield is controlled by the radiation imposed by the earthquake and the variations in crustal and upper-mantle structure along the propagation paths. Thus, to predict strong-ground-motion behavior for future events we need a good understanding of the details of their 3D structures.

We can hope to recover such information by combining observations and numerical simulations for larger events such as the 2000 Tottori-ken Seibu earthquake. The recent development of dense strong-motion networks in Japan (K-NET and KiK-net) allows the direct visualization of the wave field generated during large earthquakes. At the same time, steady improvements in computer power and parallel algorithms mean that it is possible to provide realistic simulation of 3D propagation over a regional scale to 1 Hz, with inclusion of surficial structure via an embedded submesh.

For the 2000 Tottori-ken Seibu event we have been able to achieve a fairly good match between observation and computer simulation for the dominant features of the wave field, but there are still significant differences in detail. To provide a closer link to the observations we need to use more complex source-slip models and smaller-scale structure in the velocity and attenuation models. Nevertheless, the present level of agreement between observations and numerical simulations indicates that we have a very useful tool for investigating the likely pattern of strong ground motion in areas where no major events have occurred in recent times, such as western Shikoku. The use of fine-scale surficial structure provides a useful means of estimating the amplification effects for the major population centers in sedimentary basins.

Improvements in the prediction of strong-ground-motion patterns for future earthquake scenarios will depend on maintaining a close link between available observations and comparable simulations so that we can understand the complex of behavior of the regional seismic wave field as it travels through a 3D structure.

Acknowledgments

This study was supported by the Earth Simulator Project of Ministry of Education, Culture, Sports and Technology. The collaboration was initiated when B.L.N.K. visited Japan on an Invitational Fellowship from the Japan Society for the Promotion of Science. The K-NET and KiK-net data are made available by the National Institute for Earth Science and Disaster

Research (NIED), Japan. We thank Drs. Y. Yagi and M. Kikuchi for providing their source model. We also thank to Drs. R. Harris and F. Pollitz for constructive comments that improved the manuscript.

Supplementary materials comprising the MPEG Movies for both observed wave propagation and numerical simulation (Figs. 2 and 7) can be viewed at the SSA web site (http://www.seismosoc.org).

References

Aoi, S., and H. Fujiwara (1999). 3-D finite-difference method using discontinuous grids, *Bull. Seism. Soc. Am.* **89,** 918–930.

Aoi, S., S. Obara, S. Hori, K. Kasahara, and Y. Okada (2000). New strong-motion observation network: KiK-net, *EOS Trans. Am. Geophys. Union* **81,** F863.

Carroll, D. L. (1996). Genetic algorithms and optimizing chemical oxygen-iodine lasers, in *Developments in Theoretical and Applied Mechanics*, H. B. Wilson, R. C. Batra, C. W. Bert, A. M. J. Davis, R. A. Schapery, D. S. Stewart, and F. F. Swinson (Editors) XVIII, School of Engineering, The University of Alabama, Tuscaloosa.

Friederich, W., E. Wielandt, and S. Stange (1994). Non-plane geometries of seismic surface wavefields and their implications for regional surface-wave tomography, *Geophys. J. Int.* **119,** 931–948.

Furumura, T., and B. L. N. Kennett (2001). Variations in regional phase propagation in the area around Japan, *Bull. Seism. Soc. Am.* **91,** 667–682.

Furumura, T., K. Koketsu, and H. Takenaka (2000). A hybrid PSM/FDM parallel simulation for 3-D seismic (acoustic) wavefield, *Butsuri-Tanka* (*J. SEGI*) **53,** 294–308.

Furumura, T., K. Koketsu, and K.-L. Wen (2002), Parallel PSM/FDM hybrid simulation of ground motions from the 1999 Chi-Chi, Taiwan, earthquake, *Pure Appl. Geophys.* **159,** 2133–2146.

Horikawa, H. (2000). Source process of the 2000 Tottori-ken Seibu earthquake, http://www.gsj.go.jp/horikawa/2000Tottori/source.html.

Huang, B.-S. (2000). Two-dimensional reconstruction of the surface ground motions of an earthquake: the September 21, 1999, Chi-Chi, Taiwan, Earthquake, *Geophys. Res. Lett.*, **27,** 3025–3028.

Ikeda, M., and T. Sasatani (1991). A study of site effects by means of strong motion records from intermediate depth earthquakes: Kyushu distinct, *Zishin* **44,** 233–246.

Ito, K., K. Matsumura, J. Wada, M. Joramp, S. Nakao, T. Shibutani, K. Nishigami, H. Katao, F. Takeuchi, K. Watanebe, H. Watanabe, and H. Negishi (1995). Seismogenic layer of the crust in the inner zone of southwest Japan, Annuals, Disast. Prev. Res. Inst., Kyoto Univ. **38 B-1,** 209–219.

Iwata, T., H. Sekiguchi, and K. Irikura (2000). Source process of the 1999 Chi-Chi, Taiwan, earthquake and simulation of near-source strong ground motions, *Abst. Seism. Soc. Japan 2000 Fall Meet.*, **B18**.

Kennett, B. L. N., and T. Furumura (2002). The influence of 3-D structure on the propagation of seismic waves away from earthquakes, *Pure Appl. Geophys.* **159,** 2113–2131.

Kinoshita, S. (1998). Kyoshin Net (K-NET), *Seism. Res. Lett.* **69,** 309–332.

Koketsu, K., and Kikuchi, M. (2000). Propagation of seismic ground motion in the Kanto basin, Japan, *Science* **288,** 1237–1239.

Liu, H.-L., and D. V. Helmberger (1985). The 23;19 aftershocks of the 15 October 1975 Imperial Valley earthquake: more evidence for an asperity, *Bull. Seism. Soc. Am.* **75,** 689–708.

Liu, K.-S., T.-C. Shin, and Y.-B. Tsai (1999). A free-field strong motion network in Taiwan: TSMIP, *TAO* **10,** 377–396.

Nafe, J. E., and C. L. Drake (1957). Physical properties of marine sediments, in *The Sea*, M. N. Hill (Editor), Vol. 3, Interscience, New York, 794–815.

Ryoki, K. (1999). Three-dimensional depth structure of the crust and uppermost mantle beneath Southwestern Japan and its regional gravity anomalies, *Zishin* **52,** 51–63.

Shibutani, T., A. Tada, and K. Hirahara (2000). Crust and slab structure beneath Shikoku and the surrounding area inferred from receiver function analysis in *Abst. Seism. Soc. Japan 2000 Fall Meet.*, Tsukuba, 11–13 November, **B51**.

Shima, H. (1962). On the velocity of Lg waves in Japan, *Q. J. Seismol.* **21,** 107–111.

Smith, W. H. F., and P. Wessel (1990). Gridding with continuous curvature splines in tension, *Geophysics* **55,** 293–305.

Tsuboi, C. (1954). Determination of the Gutenberg-Richter's magnitude of earthquakes occurring in and near Japan, *Zisin* **7,** 185–193.

Utsu, T. (1958). On the *Lg* phase of seismic waves observed in Japan, *Q. J. Seismol.* **23,** 61–76.

Wang, Y., J. Xu, and G. T. Schuster (2001). Viscoelastic wave simulation in basins by a variable-grid finite-difference method, *Bull. Seism. Soc. Am.* **91,** 1741–1749.

Wielandt, E. (1993). Propagation and structural interpretation of non-plane waves, *Geophys. J. Int.* **113,** 45–53.

Yagi, Y., and M. Kikuchi (2000). Source rupture process of the Tottori-ken Seibu earthquake of Oct. 6, 2000, (Mjma 7.3) by using joint inversion of far-field and near-field waveform, in *Abst. Seism. Soc. Japan 2000 Fall Meet.*, Tsukuba, 11–13 November, **T04**.

Yamazaki, F., and T. Ooida (1985). Configuration of subducted Philippine Sea plate beneath the Chubu distinct, central Japan, *Zishin* **38,** 193–201.

Yoshii, A., K. Koketsu, and D. Zhad (2002). S wave tomography beneath Japan Islands, *Abst. Japan Earth and Planet. Sci. Joint Meet.*, SZ-P002.

Yoshii, T., Y. Sasaki, T. Tada, H. Okada, A. Shuzo, I. Muramatu, I. Hashizume, and T. Moriya (1974). The third Kurayoshi explosion and the crustal structure in western part of Japan, *J. Phys. Earth* **22,** 109–121.

Zhao, D. A., and A. Hasegawa (1993). P wave tomographic imaging of the crust an upper mantle beneath the Japan Islands, *J. Geophys. Res.* **98,** 4333–4353.

Earthquake Research Institute
University of Tokyo
1-1-1 Yayoi, Bunkyo-ku
Tokyo 113-0032, Japan
(T.F., K.K.)

Research School of Earth Sciences
Australian National University
Canberra ACT 0200, Australia
(B.L.N.K.)

Manuscript received 16 July 2002.